Scattering-Parameter Models and Representations for Microwave Mixers

Dylan F. Williams, *Fellow, IEEE*, Fabien Ndagijimana, Kate A. Remley, *Member, IEEE*, Joel A. Dunsmore, *Member, IEEE*, and Sean Hubert

***Abstract*—We present straightforward models and representations for RF and image mixers, and develop simple rules for transforming electrical problems involving mixers and signals at several frequencies into equivalent single-frequency problems. We show how those models, representations, and rules can be applied to mixer characterization with vector network analyzers, and how they relate to more general descriptions based on scattering parameters currently in use.**

***Index Terms*—Frequency conversion, frequency translation, image frequency, microwave, mixer, model, scattering parameters.**

I. Introduction

We develop system-level models and representations for electrical mixers based on scattering parameters and ideal mixer blocks. The scattering parameters describe the reflections, transfer function, and degree of reciprocity of the mixers. The ideal mixer blocks describe their ideal frequency-translation behavior. Results from the experimental study of [1], some of which we present here, confirm the theory.

An electrical mixer multiplies a low-level input signal at one of its ports by a high-level local-oscillator (LO) signal at frequency $\omega_{\rm LO}$. This multiplication is accomplished by using the high-level LO signal to periodically turn on and off diodes (or transistors) in the mixer, creating a time-varying conductance with the same periodicity as the LO signal. The circuit is designed so that the time-varying conductance modulates (multiplies) the low-level input signal. This temporal multiplication translates low-level signals between a (typically) low intermediate frequency (IF) $\omega_{\rm IF}$ at one port of the mixer and signals at an "RF" frequency $\omega_{\rm RF} = \omega_{\rm LO} + \omega_{\rm IF}$ or an "image" (IM) frequency $\omega_{\rm IM} = \omega_{\rm LO} - \omega_{\rm IF}$ at the other port of the mixer.

Electrical mixers also generate a number of other "mixing products" (additional or "spurious" frequency components) at sums and differences of the harmonics of the LO, IF, RF, and image frequencies. References [2] and [3] outline a complete circuit theory describing this behavior, which we do not address here, in terms of conversion matrices.

The conversion matrices of [2] and [3], which we summarize in Appendix I, express the relationships between voltages and currents or, equivalently, the forward and backward waves at all of the frequencies generated by a mixer. While the theories of [2] and [3] are essential for mixer design, they are more complex than required for most system-level design. This complexity, as well as the integration of the frequency-translating properties of the mixer into the conversion matrices themselves, obscures some important relationships and makes them difficult to use for systems design and test.

In practice, most mixers are operated as simple frequency converters in a quasi-linear regime. They are configured with strong LO, small-signal inputs, and filters that allow up- and down-conversion between the mixer's IF and RF frequency, and do not create spurious signals at other frequencies. We call these standard RF mixers. We call like mixers that only allow up- and down-conversion between the IF and image frequencies "image" mixers.

Here, we restrict our discussion to standard RF and image mixers satisfying these restrictions. Specifically, we ignore any spurious mixer outputs at other frequencies, and do not treat issues such as mixer nonlinearity or dependence on the level of the LO signal. By restricting ourselves to a single frequency at each port, and separating the frequency-translating behavior of the mixer from its nonideal behavior, we are able to develop models and representations that clarify system-level mixer behavior. In particular, we develop a set of straightforward and intuitive rules for transforming multifrequency mixer problems into equivalent single-frequency problems that can be solved with the simplest computer-aided-design software tools or even analytically in many cases. The rules we develop find immediate application in the characterization of mixers with vector network analyzers (VNAs). In Appendices I and II, we relate our representations to conversion matrices and large-signal scattering functions.

II. Basic Mixer Operation

The trigonometric identity $\cos(A)\cos(B) = 1/2[\cos(A + B) + \cos(A - B)]$ helps us to understand the basic operation of an electrical mixer in the time and frequency domains. For example, we can replace A in the identity with the total phase $\omega_{\rm LO}t + \theta_{\rm LO}$ of a sinusoidal signal at the LO port, and B in the identity with the total phase $\omega_{\rm IF}t + \theta_{\rm IF}$ of a sinusoidal signal at the IF port. This shows that the multiplication in time of the LO and IF signals in a mixer results in two new frequency components at the RF (sum) frequency with total phase $\omega_{\rm RF}t + \theta_{\rm RF} = (\omega_{\rm LO} + \omega_{\rm IF})t + (\theta_{\rm LO} + \theta_{\rm IF})$ and image (difference) frequency with total phase $\omega_{\rm IM}t + \theta_{\rm IM} = (\omega_{\rm LO} - \omega_{\rm IF})t + (\theta_{\rm LO} - \theta_{\rm IF})$.

Fig. 1 shows how the phases and, in a like manner, the frequencies of the LO, IF, RF, and image frequencies are related. The horizontal arrows illustrate how an increase or decrease in

Manuscript received January 5, 2004; revised February 21, 2004.

D. F. Williams and K. A. Remley are with the National Institute of Standards and Technology, Boulder, CO 80305 USA (e-mail: dylan@boulder.nist.gov).

F. Ndagijimana is with the Institut Universitaire de Technologie, Université Joseph Fourier, 38041 Grenoble, France.

J. A. Dunsmore and S. Hubert are with the Component Test Division, Agilent Technologies, Santa Rosa, CA USA.

Digital Object Identifier 10.1109/TMTT.2004.839917

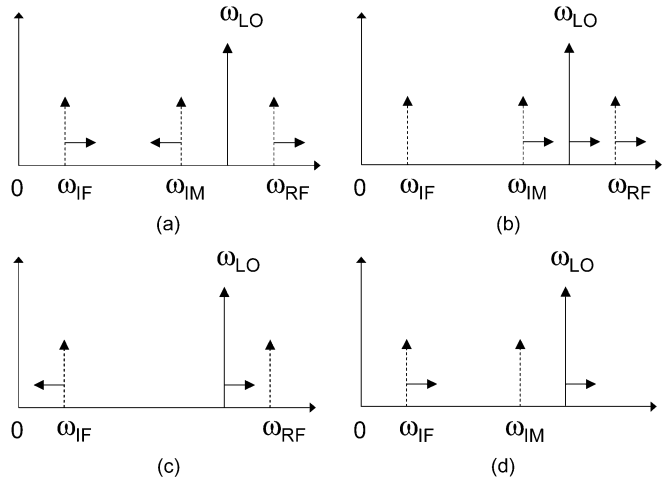

Fig. 1. Frequencies at the input and output of an electrical mixer. The horizontal arrows show how changes in the phase or frequency of an input signal change the output signal. (a) Changing IF, RF, or IM and fixed LO. (b) Fixed IF and changing LO. (c) Fixed RF and changing LO. (d) Fixed IM and changing LO.

the phase (or frequency) of one of the input sinusoids to the mixer changes the phase (or frequency) of the mixer's output sinusoid. For example, Fig. 1(a) indicates that an increase in the phase of the input sinusoid at the IF will increase the phase of an output sinusoid at the RF, but *decrease* the phase of an output sinusoid at the image frequency.

We take special care to treat image mixers in our development. We will see later that the phase reversal of the IF and image signals complicates the electrical behavior of image mixers at their output ports.[1]

III. Standard RF Mixer

Conventional scattering parameters (i.e., the pseudowave scattering parameters of [4]) can be used to describe the electrical behavior of linear time-invariant electrical two-ports. The conventional scattering parameters S_{ij} relate the incident and reflected wave coefficients a_1 and b_1 at port 1 of the device to the incident and reflected wave coefficients a_2 and b_2 at port 2 of the device by

$$\begin{bmatrix} b_1 \\ b_2 \end{bmatrix} = \begin{bmatrix} S_{11} & S_{12} \\ S_{21} & S_{22} \end{bmatrix} \begin{bmatrix} a_1 \\ a_2 \end{bmatrix}. \tag{1}$$

The requirement that the frequencies on the two ports are the same is an important restriction on (1).

The ideal RF mixer of Fig. 2(a) acts purely as a frequency translator. Choosing the reference impedance [4] as real, the incident and reflected wave coefficients $a_{\rm IF}$ and $b_{\rm IF}$ at frequency $\omega_{\rm IF}$ on the IF port of the ideal RF mixer are related to the incident and reflected wave coefficients $a_{\rm RF}$ and $b_{\rm RF}$ at frequency $\omega_{\rm RF} = \omega_{\rm LO} + \omega_{\rm IF}$ on the RF port of the mixer by

$$\begin{bmatrix} b_{\rm IF} \\ b_{\rm RF} \end{bmatrix} = \begin{bmatrix} 0 & a_{\rm LO}^{*} \\ a_{\rm LO} & 0 \end{bmatrix} \begin{bmatrix} a_{\rm IF} \\ a_{\rm RF} \end{bmatrix} \tag{2}$$

[1]Unlike the RF mixer, we can reverse the two ports of an ideal image mixer without changing its electrical behavior. However, to avoid confusion, we assign unique labels to the two ports of the ideal image mixer. Sticking with convention, we call one port the IF port and the other the image port.

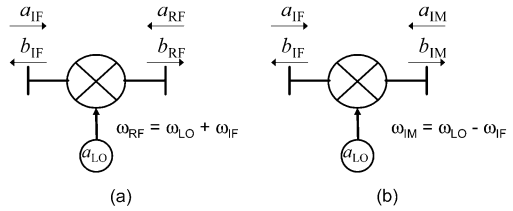

Fig. 2. Schematic and incoming and outgoing waves of an ideal mixer block. (a) RF mixer. (b) Image mixer.

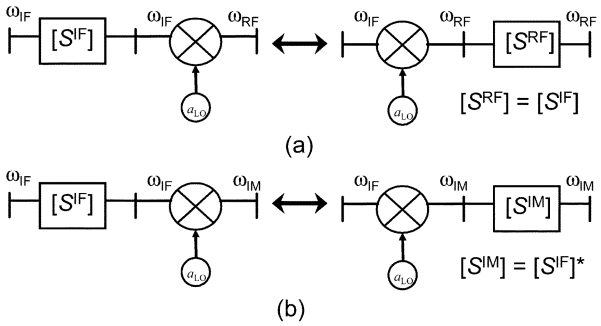

Fig. 3. Models and representations for imperfect mixers. (a) RF mixer. (b) Image mixer.

where $a_{\rm LO}$ is the wave coefficient of the LO signal at the ideal mixer, and the superscript $*$ refers to the complex conjugate, which corresponds to reversing the phase of the coefficient.

The LO power in most mixers is set at a level high enough to turn the mixing elements (the diodes or transistors) completely on and off with each cycle of the LO. Thus, to first order, an increase or decrease in LO power does not change the mixer output. Thus, we set $|a_{\rm LO}| = 1$.

Equation (2) can be understood by referring to Fig. 1. We see that increasing the phase of the incident-wave coefficient $a_{\rm IF}$ at the IF port or the phase $a_{\rm LO}$ of the LO increases the phase of the outgoing-wave coefficient $b_{\rm RF}$ at the RF port, as shown in Fig. 1(a) and (b). Likewise, increasing the phase of $a_{\rm RF}$ or decreasing the phase of $a_{\rm LO}$ increases the phase of $b_{\rm IF}$, as illustrated in Fig. 1(a) and (c).

Note that because the frequencies at the IF and RF ports of the ideal mixer are not the same, the electrical behavior of even this ideal RF mixer cannot be represented by a conventional scattering-parameter matrix. The matrix in (2) is perhaps more appropriately called a conversion matrix [5], but should not be confused with the more general conversion matrices described in [2] and [3].

Of course, no mixer is ideal: real mixers have a frequency-dependent conversion loss (or gain) and phase distortion that we will attempt to capture in our mixer representation. However, we will ignore a number of second-order nonlinear effects.

Fig. 3(a) shows two models or representations of a nonideal RF mixer. In these mixer models, we separate the ideal frequency-translating behavior of the mixer from its nonideal behavior, which we represent in terms of standard scattering parameters.

In the first model, all of the nonideality of the mixer caused by reflections, imperfect conversion loss, and phase distortion is described by a scattering-parameter matrix $[S^{\rm IF}]$ placed before

the ideal mixer block. Here, $[S^{\mathrm{IF}}]$ relates the wave coefficients at its two ports by (1), and those waves have the same frequency ω_{IF}. It is the ideal mixer block to the right of $[S^{\mathrm{IF}}]$, whose electrical behavior is described by (2), that performs the frequency translation between the IF and RF frequencies. Thus, we can call $[S^{\mathrm{IF}}]$, which is akin to an "error box" used to describe nonidealities in VNAs, a true scattering-parameter matrix.

In the second model, the nonideality of the mixer is described by a similar scattering-parameter matrix $[S^{\mathrm{RF}}]$ placed after the ideal mixer block. While $[S^{\mathrm{RF}}]$ relates wave coefficients with frequency ω_{RF}, rather than ω_{IF}, the frequencies are still the same at both ports of $[S^{\mathrm{RF}}]$ so we can also call $[S^{\mathrm{RF}}]$ a true scattering-parameter matrix.

From (1) and (2), we can readily show that, for nonideal RF mixers

$$\begin{bmatrix} b_{\mathrm{IF}} \\ b_{\mathrm{RF}} \end{bmatrix} = \begin{bmatrix} S_{11}^{\mathrm{IF}} & a_{\mathrm{LO}}^{*} S_{12}^{\mathrm{IF}} \\ a_{\mathrm{LO}} S_{21}^{\mathrm{IF}} & S_{22}^{\mathrm{IF}} \end{bmatrix} \begin{bmatrix} a_{\mathrm{IF}} \\ a_{\mathrm{RF}} \end{bmatrix} = \begin{bmatrix} S_{11}^{\mathrm{RF}} & a_{\mathrm{LO}}^{*} S_{12}^{\mathrm{RF}} \\ a_{\mathrm{LO}} S_{21}^{\mathrm{RF}} & S_{22}^{\mathrm{RF}} \end{bmatrix} \begin{bmatrix} a_{\mathrm{IF}} \\ a_{\mathrm{RF}} \end{bmatrix}. \quad (3)$$

The matrices in (3) incorporate the frequency-translating behavior of the mixers, and are similar in form of the conversion matrices discussed in [2] and [3] (see Appendix I).

Note that the phase of a_{LO} in (3) is the phase of the LO at the ideal mixer block in the model. The phase of a_{LO} is *not* usually equal to the phase of the LO at the mixer's LO port. This distinction is important since, while the phase of the LO at the mixer's LO port is often measurable, the phase of a_{LO} is not.

Equation (3) shows that, while $[S^{\mathrm{IF}}]$ and $[S^{\mathrm{RF}}]$ relate incident and reflected waves at different frequencies, their elements are equal. Thus, we conclude that $[S^{\mathrm{IF}}] = [S^{\mathrm{RF}}]$. This important fact is summarized graphically by the two equivalent representations shown in Fig. 3(a).

We can easily show from (2) that the IF source at frequency ω_{IF} and ideal RF mixer in Fig. 4(a) can be described by an equivalent RF source at frequency ω_{RF} with source output-wave coefficient $b_{\mathrm{RF}} = a_{\mathrm{LO}} b_{\mathrm{IF}}$. Likewise, the RF source at frequency ω_{RF} and ideal RF down-converting mixer in Fig. 4(b) can be described by an equivalent IF source at frequency ω_{IF} with source output-wave coefficient $b_{\mathrm{IF}} = a_{\mathrm{LO}}^{*} b_{\mathrm{RF}}$. Finally, Fig. 5 gives the scattering parameters for two ideal "back-to-back" RF mixers.

IV. Transformation to a Single-Frequency Problem

The relations summarized in Figs. 3–5 can be regarded as a set of rules for transforming mixer problems into equivalent single-frequency problems that can be solved with conventional procedures and formulas. The idea is to use the transformations and relations in the figures to "move" the ideal mixer blocks to the left- or right-hand side and eventually combine them either with other ideal mixer blocks or with sources.

When ideal up-converters and down-converters are combined, the result is one of the two scattering-parameter matrices shown in Fig. 5. When ideal mixer blocks are combined with sources, they simply translate the phase and frequency of the source, as illustrated in Fig. 4. In either case, the ideal mixer blocks and multiple frequencies are removed from the problem.

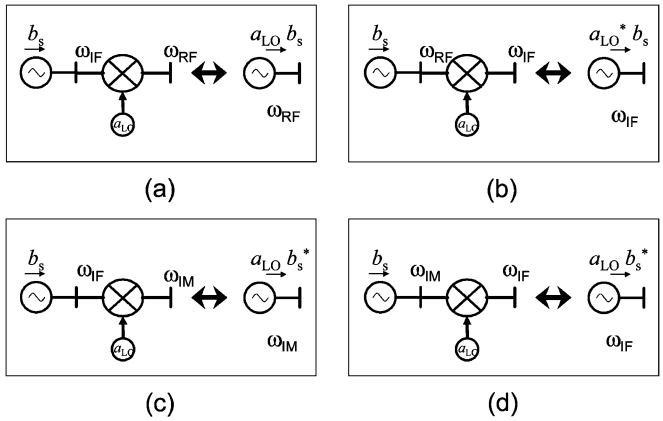

Fig. 4. Equivalent sources for RF and image mixers. (a) RF up. (b) RF down. (c) Image up. (d) Image down.

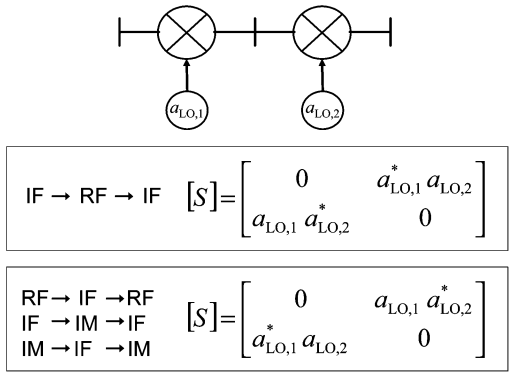

Fig. 5. Scattering parameters of two cascaded mixers with the same LO frequency. The top box shows the scattering parameters of a mixer cascade that translates signals from the IF to the RF and back to the IF frequency. The bottom box shows the scattering parameters of three other common configurations.

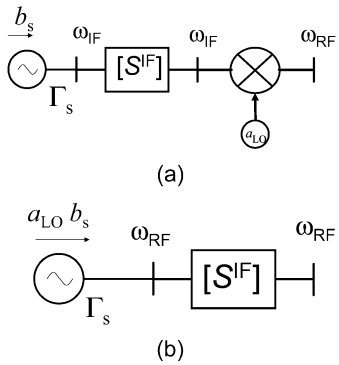

Fig. 6. Actual and equivalent circuit for a source and RF mixer. (a) Actual circuit. (b) Equivalent circuit at RF frequency.

Fig. 6 illustrates the application of the procedure to an example incorporating a standard RF mixer. Due to the RF mixer in the circuit, we cannot solve for the electrical behavior of the circuit of Fig. 6(a) with conventional scattering-parameter rules.

However, we can use the relationship summarized in Fig. 3(a) to interchange the position of $[S^{\mathrm{IF}}]$ and the ideal mixer in the

circuit. By splitting the source into an ideal matched source and a scattering-parameter "error box" of the form

$$[S_\Gamma] = \begin{bmatrix} 0 & 0 \\ 1 & \Gamma_S \end{bmatrix} \tag{4}$$

we can then move the ideal mixer through the source reflection coefficient. Finally, we can use the relationship of Fig. 4(a) to combine the ideal RF mixer and source, which gives us the equivalent circuit of Fig. 6(b).

We have now transformed the problem of Fig. 6(a), which contains signals at both the IF and RF frequencies, into the single-frequency problem at the RF frequency of Fig. 6(b).

V. Image Mixer

The rules and transformations for standard RF mixers we discussed in Section IV were quite straightforward. Now we address the more complicated case of the image mixer.

Fig. 2(b) shows an ideal image mixer. The incident and reflected wave coefficients $a_{\rm IF}$ and $b_{\rm IF}$ at frequency $\omega_{\rm IF}$ on the IF port are related to the incident and reflected wave coefficients $a_{\rm IM}$ and $b_{\rm IM}$ at the *difference* frequency $\omega_{\rm IM} = \omega_{\rm LO} - \omega_{\rm IF}$ on the image port of the mixer with

$$\begin{bmatrix} b_{\rm IF} \\ b^*_{\rm IM} \end{bmatrix} = \begin{bmatrix} 0 & a_{\rm LO} \\ a^*_{\rm LO} & 0 \end{bmatrix} \begin{bmatrix} a_{\rm IF} \\ a^*_{\rm IM} \end{bmatrix}. \tag{5}$$

Fig. 1 also helps us to understand (5). For example, we see that increasing the phase of the incident-wave coefficient $a_{\rm IF}$ at the IF port *decreases* the phase of the outgoing-wave coefficient $b_{\rm IM}$ at the image port, as illustrated in Fig. 1(a). This explains why the conjugate $b^*_{\rm IM}$ of $b_{\rm IM}$, and not $b_{\rm IM}$, appears in (5).

The consequences of the conjugates on $a_{\rm IM}$ and $b_{\rm IM}$ in (5) are profound: (5) cannot be rewritten in the form of (1) describing the way in which conventional scattering parameters relate incident and reflected waves. This is because *increasing* the phase of an incident wave on an image mixer *decreases* the phase of the output wave at the other port. Conventional scattering parameters, on the other hand, force the phase of the output to increase when the phase of the input is increased. Thus, we see that, while (5) is fairly straightforward, its form differs fundamentally from that of (1).

From (1) and (5), it is easy to show that, for a nonideal image mixer

$$\begin{aligned} \begin{bmatrix} b_{\rm IF} \\ b^*_{\rm IM} \end{bmatrix} &= \begin{bmatrix} S^{\rm IF}_{11} & a_{\rm LO} S^{\rm IF}_{12} \\ a^*_{\rm LO} S^{\rm IF}_{21} & S^{\rm IF}_{22} \end{bmatrix} \begin{bmatrix} a_{\rm IF} \\ a^*_{\rm IM} \end{bmatrix} \\ &= \begin{bmatrix} S^{\rm IM*}_{11} & a_{\rm LO} S^{\rm IM*}_{12} \\ a^*_{\rm LO} S^{\rm IM*}_{21} & S^{\rm IM*}_{22} \end{bmatrix} \begin{bmatrix} a_{\rm IF} \\ a^*_{\rm IM} \end{bmatrix}. \end{aligned} \tag{6}$$

Thus, the two equivalent-circuit models of the image mixer in Fig. 2 are related by $[S^{\rm IF}] = [S^{\rm IM}]^*$. The conjugation of the scattering parameters in $[S^{\rm IM}]$ is related to the fact that, like the standard RF mixer, the ideal image mixer is not time invariant, and arises from the conjugates on $a_{\rm IM}$ and $b_{\rm IM}$ in (5).

From the relation $[S^{\rm IF}] = [S^{\rm IM}]^*$, we see that interchanging the position of an ideal image mixer and conventional scattering-parameter matrix, as illustrated in Fig. 3(b), conjugates all of the elements of those scattering parameters. This is no trick as we have ever seen ordinary scattering parameters perform before, and illustrates how profoundly (5) differs from (1).

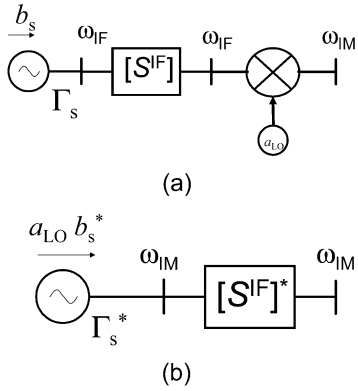

Fig. 7. Actual and equivalent circuit for a source and an image mixer. (a) Actual circuit. (b) Equivalent circuit at image frequency.

Fig. 4(c) and (d) shows equivalent-circuit models for sources and image mixers. The similarity of the two models is not surprising given the reversibility of the two ports of an ideal image mixer.

Finally, Fig. 5 shows the scattering parameters of two cascaded mixers with the same LO frequency. For the four configurations shown in this figure, the frequencies at the input and output of the cascade are the same, and the cascade is described by a true scattering-parameter matrix.

VI. Image-Mixer Problem

We can also use the relations summarized in Figs. 3–5 to transform image-mixer problems into equivalent single-frequency problems. However, as Figs. 3–5 indicate, moving ideal image mixers through other circuits conjugates their scattering parameters.

Fig. 7 illustrates the procedure for the example of Fig. 6 with an image, rather than an RF, mixer. When we use the relationship summarized in Fig. 3(b) to interchange the position of $[S^{\rm IF}]$ and the ideal image mixer in the circuit, we conjugate $[S^{\rm IF}]$ in the process. Likewise, when we move the ideal image mixer through the source reflection coefficient, we also conjugate $\Gamma_{\rm s}$. Finally, using the relationship of Fig. 4(c) to combine the ideal image mixer and source, we obtain the equivalent circuit of Fig. 7(b). We have now transformed the problem of Fig. 7(a), which contains signals at both the IF and image frequencies, into the single-frequency problem at the image frequency of Fig. 7(b). The equivalent circuit of Fig. 7(b) can be easily simulated in computer-aided design (CAD) software or solved analytically.

VII. Mixer Reciprocity and Group Delay

Passive time-invariant circuits constructed of reciprocal materials satisfy the Lorentz reciprocity theorem, and are often called "reciprocal." Reciprocity in this sense implies that the circuits forward and reverse transmission coefficients S_{21} and

S_{12} are equal. Implicit in this statement is the fact that the input and output frequencies of the circuit are equal.

Obviously, microwave mixers do not satisfy the requirements of the Lorentz reciprocity theorem and, thus, would not be expected, in general, to be reciprocal. In fact, even an ideal RF mixer whose electrical behavior is defined by (2) is not reciprocal in any strict sense since the relationships between its input and output phases depend on the LO frequency, i.e., we can always choose $a_{\rm LO}$ in (2) so as to set the difference of the phase of $b_{\rm IF}/a_{\rm RF}$ and $b_{\rm RF}/a_{\rm IF}$ equal to any value we desire.

How then are we to define the reciprocity of a mixer? Perhaps the best way to define mixer reciprocity is not in terms of the mixer itself, but rather in terms of the scattering parameters $[S^{\rm IF}]$ defining the lack of ideality of the mixer. Not only do these scattering parameters relate input and output wave coefficients at the same frequency and, thus, might actually be capable of being reciprocal in the conventional sense, but stating that $S_{21}^{\rm IF} = S_{12}^{\rm IF}$ guarantees us that signals are distorted during up- and down-conversion in the same way, which corresponds to what we intend to say when we claim that a mixer is reciprocal.

The difference in magnitudes of $S_{21}^{\rm IF}$ and $S_{12}^{\rm IF}$ can be determined in a straightforward way from measurements with traceable power calibrations [5]–[7]. However, in most measurement situations, we will be able to measure the phases of the ratios $b_{\rm IF}/a_{\rm RF}$ and $b_{\rm RF}/a_{\rm IF}$ (and, thus, $a_{\rm LO}^* S_{21}^{\rm IF}$ and $a_{\rm LO} S_{12}^{\rm IF}$) and the phase of the LO at the mixer port, but not the phase of $a_{\rm LO}$ at the ideal mixer block in the model. This is true when making measurements with oscilloscopes and three-port large-signal network analyzers [7]. In some VNA measurements [3], we cannot even measure the phase of the LO at the mixer port, much less the phase of $a_{\rm LO}$ at the ideal mixer block in the model. Thus, in all of these situations, we are only able to measure the difference of $S_{21}^{\rm IF}$ and $S_{12}^{\rm IF}$ to within an unknown constant equal to twice the phase of the unknown LO phase at the ideal mixer.

Since we are only able from measurements at the ports of a mixer to determine the difference of the phases of $S_{21}^{\rm IF}$ and $S_{12}^{\rm IF}$ to within an unknown constant, we must content ourselves with defining mixer reciprocity, or the lack of it, in terms of the *changes* in the phases of $S_{21}^{\rm IF}$ and $S_{12}^{\rm IF}$ with frequency. The group delay $t_{\rm g}$ is a measure of the time a band-limited signal takes to pass through an electrical system, and is an ideal way to describe mixer reciprocity.

Group delay is defined by $t_{\rm g} = -d\phi/d\omega$, where ϕ is the electrical phase of the signal at the output of the network minus the electrical phase of the signal at the input of the network at the same frequency. In our context, we can define the forward and backward group delay of the mixer in terms of the phases of $S_{21}^{\rm IF}$ and $S_{12}^{\rm IF}$ measured at a fixed value of $a_{\rm LO}$. Note that the group delay $t_{\rm g}$ does not depend on the absolute phase of the transfer function, which, in turn, depends on the absolute phase of $a_{\rm LO}$ and, thus, offers an ideal way of expressing the phase reciprocity of a mixer.

As we noted above, group delay is calculated from the transfer function of a system whose input and output signals are at the same frequency. The rules we developed here for translating multifrequency mixer problems into single-frequency problems are, thus, ideal aids in calculating the group delay of circuits containing mixers.

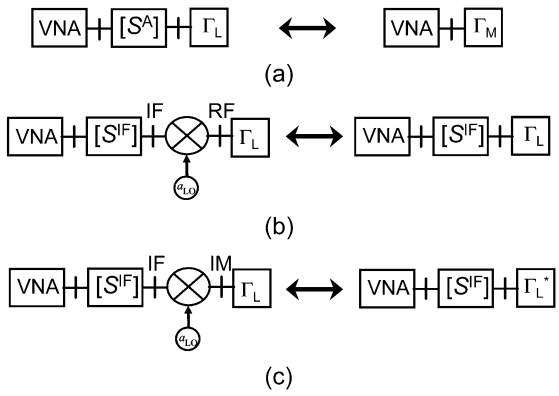

Fig. 8. Equivalent circuits for junction and mixer characterization with a VNA. (a) Microwave junction. (b) RF mixer. (c) Image mixer.

VIII. Mixer Characterization With a VNA

We now turn our attention to experimental results obtained from VNA measurements that illustrate the rules we have introduced for image mixers. Bauer and Penfield introduced a classic method of determining the scattering parameters of microwave junctions in [8]. They began by connecting one port of the microwave junction with unknown scattering parameters $[S^{\rm A}]$ to a calibrated VNA, as shown schematically in Fig. 8(a). They then connected a load with a known reflection coefficient $\Gamma_{\rm L}$ to the other port of the junction, and used the VNA to measure the reflection coefficient of the junction and its terminating load.

The reflection coefficient $\Gamma_{\rm M}$ of the combination of the junction and its load, as measured by the VNA, is given by

$$\Gamma_{\rm M} = S_{11}^{\rm A} + \frac{S_{12}^{\rm A} S_{21}^{\rm A} \Gamma_{\rm L}}{1 - S_{22}^{\rm A} \Gamma_{\rm L}}. \tag{7}$$

Bauer and Penfield noted that three such measurements are sufficient to determine $S_{11}^{\rm A}, S_{22}^{\rm A}$ and the product $S_{12}^{\rm A} S_{21}^{\rm A}$, and developed a least squares solution to make optimal use of a greater number of measurements when they were available. Finally, for passive junctions comprised entirely of reciprocal materials, Bauer and Penfield noted that $S_{12}^{\rm A} = S_{21}^{\rm A}$, allowing $S_{12}^{\rm A}$ and $S_{21}^{\rm A}$ to be determined from the measured product $S_{12}^{\rm A} S_{21}^{\rm A}$.

Dunsmore [5] adapted this idea to RF mixer characterization using the measurement configuration sketched on the left-hand side of Fig. 8(b). Dunsmore noted that (7) also applied to the RF mixer's scattering parameters $[S^{\rm IF}]$. He used a variant of the classic procedure pioneered by Bauer and Penfield to solve for $[S^{\rm IF}]$ from a set of $\Gamma_{\rm M}$ measurements of the reflection coefficient of the mixer terminated with different loads with the known reflection coefficient $\Gamma_{\rm L}$. Dunsmore then assumed $S_{12}^{\rm IF} = S_{21}^{\rm IF}$ to determine $S_{12}^{\rm IF}$ and $S_{21}^{\rm IF}$ from the measured product $S_{12}^{\rm IF} S_{21}^{\rm IF}$.[2]

We can understand this procedure in the context of our mixer models and rules. First, we note that the electrical behavior of

[2]In the case of a microwave junction, this assumption is justified by the Lorentz reciprocity theorem and the choice of real reference impedances. Reference [2] shows that purely resistive mixers with symmetric conductance waveforms are reciprocal. However, as discussed earlier, reciprocity is most certainly violated in diode mixers, although it may often be a reasonable approximation.

a load can be represented with a scattering-parameter matrix of the form

$$[S_\Gamma] = \begin{bmatrix} \Gamma_\mathrm{L} & 0 \\ 0 & 0 \end{bmatrix}. \tag{8}$$

Now we can use the rule illustrated in Fig. 3(a) to "move" the ideal RF mixer block in Fig. 8(b) through the load Γ_L, leaving its reflection coefficient unchanged. The result is the equivalent circuit of Fig. 8(b). Not only has the ideal mixer block dropped out of the equivalent circuit of Fig. 8(b), but the effect of the LO phase has "cancelled" itself out completely and no longer appears in the circuit equations.

In this VNA setup, the resulting circuit in Fig. 8(b) is identical to that of Fig. 8(a) with the adapter scattering parameters $[S^\mathrm{A}]$ replaced by $[S^\mathrm{IF}]$. This explains why the mixer and its LO can be treated as a simple time-invariant two-port and justifies the application of (7) and the standard deembedding methods used to characterize microwave junctions to standard RF mixers.

We can apply the same procedure to an image mixer. However, for an image mixer, we must use the rule of Fig. 3(b) to move the ideal mixer block through the reflection coefficient Γ_L of the load, conjugating Γ_L in the process, as shown in Fig. 8(c). Thus, we see that, for image mixers, we can indeed apply the classic deembedding procedures of Bauer and Penfield and others, but must replace the reflection coefficient Γ_L of the load by Γ_L^* in the equations.

We performed three fundamental checks of this result using the measurement methods developed in [1]. In each experiment, we compared the method of [5] applied to an image mixer using both Γ_L and Γ_L^* with an independent measurement.

A. Image Mixer and a Precision Airline

We first characterized an image mixer with the method of [5]. We then added a 5-cm precision airline to the output port of the mixer and repeated the characterization. The measured loss of the airline was approximately 0.05 dB and its measured reflection coefficient was less than −45 dB so we expect the addition of the airline to modify the phase response of the image mixer while leaving its magnitude response nearly identical.

The two solid lines in Fig. 9 show the transmission coefficients obtained for the image mixer and mixer/airline combination using Γ_L^* in the calculations, as derived from our theory. The measurements differ by only approximately 0.05 dB.

However, when we performed the calculations using Γ_L, rather than Γ_L^*, we obtained the transmission coefficients denoted by dashed lines in this figure. The large discrepancy between the results we obtain using Γ_L in the calculations clearly illustrates the importance of replacing Γ_L by Γ_L^* when applying the method of [5] to the characterization of image mixers.

B. Termination in a Precision Load

We next terminated an image mixer in a precision load and used a conventionally calibrated VNA to measure the reflection coefficient of the mixer at its unterminated port. This reflection coefficient is, by definition, the reflection coefficient of the mixer at the unterminated port.

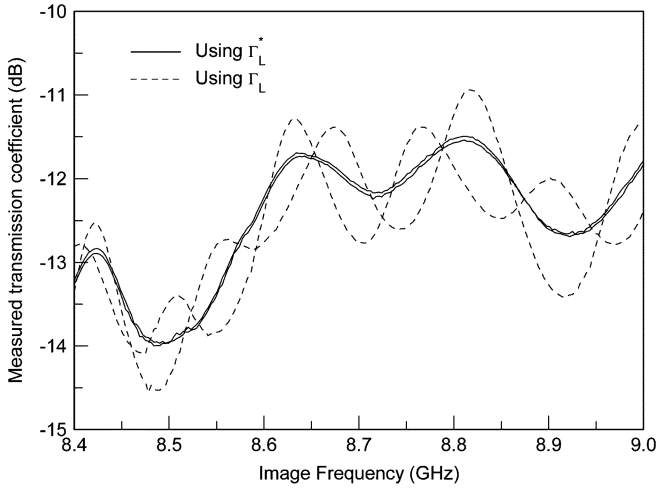

Fig. 9. VNA measurement of the transmission coefficients of an image mixer and mixer/airline combination using the method of [5]. This figure shows that Γ_L must be replaced by Γ_L^* in the method of [5] to yield results consistent with the low loss and reflection coefficient of the precision airline we used in the experiment. We used an LO frequency of 9.9 GHz and the IF frequencies spanned 0.9–1.5 GHz (data from [1]).

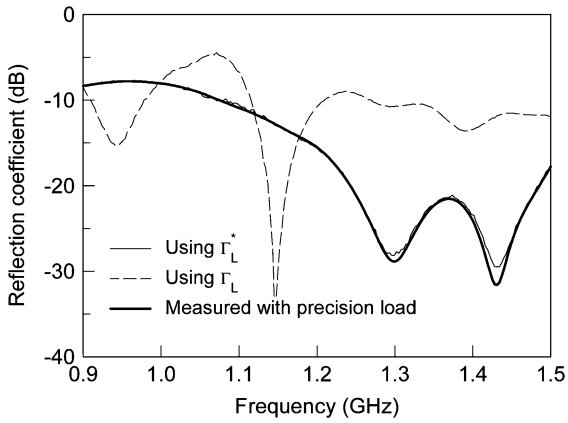

Fig. 10. VNA measurement of the reflection coefficients of an image mixer and mixer/airline combination using the method of [5]. This figure shows that Γ_L must be replaced by Γ_L^* in the method of [5] to yield results consistent with a direct measurement of the reflection coefficient of the mixer terminated with a precision resistor. We used the same frequency setting in Fig. 9 and the data was measured as described in [1] and [5].

Fig. 10 compares the reflection coefficients determined with the method of [5] using Γ_L and Γ_L^* to this more fundamental measurement of the reflection coefficient of the image mixer. This figure again shows that Γ_L must be conjugated when applying the method of [5] to image mixers.

C. Power-Meter-Calibrated Measurements

Finally, we used a power meter to directly calibrate our VNA measurements in an absolute sense at both the IF and image frequencies, and then measured the magnitudes of the forward and reverse transfer function of an image mixer directly. Fig. 11 plots the ratios of the transmission coefficients determined using the method of [5] to the mean of the directly measured forward and reverse transmission coefficients. This figure shows that using Γ_L^* in the method of [5] to characterize an image mixer yields agrees more closely with measurements performed by our power-meter-calibrated VNA than using Γ_L.

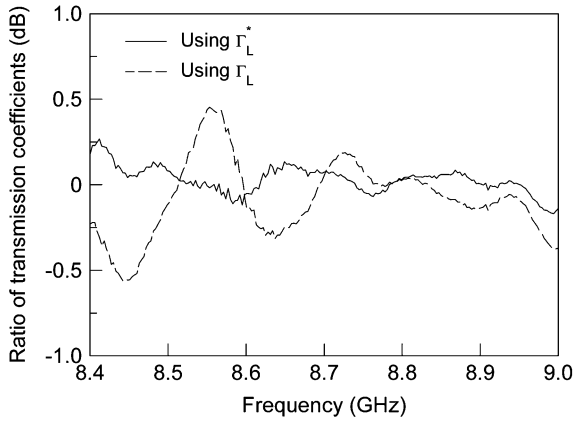

Fig. 11. Ratio of the transmission coefficients of an image mixer using the method of [5] to direct power-meter-calibrated measurements. We used the same frequency settings as for the data in Fig. 9 and the measurements were performed as described in [1] and [5].

IX. Conclusion

We have presented models and representations for standard RF mixers and image mixers based on scattering parameters and ideal mixing blocks. These models are easily incorporated into conventional computer-aided-design tools and are suitable for systems-level analysis. We have also developed a set of simple rules for analytically transforming electrical problems involving mixers and signals at several frequencies into equivalent single-frequency problems. Finally, we have shown how those models, representations, and rules can be applied to mixer characterization with VNAs. We have confirmed the theory with the experimental method described in [1].

The models and representations we have developed are limited to mixers with a single-frequency IF port and a single-frequency RF or image port. In Appendices I and II, we show how our representations are related to two more general representations based on scattering parameters applicable to a broader class of mixer and nonlinear problems.

Appendix I
Relationship to Conversion Matrices

Torrey *et al.* [2] introduced the notion of conversion matrices to describe the behavior of diode mixers in 1948. These complete conversion matrices are required for accurate mixer design, and are capable of describing spurious mixer outputs at frequencies other than the IF, RF, and image frequencies.

Maas summarized the approach of Torrey *et al.* in [3], and defined an "S matrix," which we will call S^{M}, from $S^{\mathrm{M}} \equiv (1+Y_n)^{-1}(1-Y_n)$, where Y_n is the diode's conversion (admittance) matrix. Identifying Maas' port 0 with the mixer's IF port and Maas' port 1 with the mixer's RF port, we can rewrite [3, eq. (4.87)] for an RF mixer as

$$\begin{bmatrix} b_{\mathrm{IF}} \\ b_{\mathrm{RF}} \end{bmatrix} = \left[S^{\mathrm{M,RF}}\right] \begin{bmatrix} a_{\mathrm{IF}} \\ a_{\mathrm{RF}} \end{bmatrix} \equiv \begin{bmatrix} S^{\mathrm{M}}_{00} & S^{\mathrm{M}}_{01} \\ S^{\mathrm{M}}_{10} & S^{\mathrm{M}}_{11} \end{bmatrix} \begin{bmatrix} a_{\mathrm{IF}} \\ a_{\mathrm{RF}} \end{bmatrix}. \tag{9}$$

Comparing (3) and (9), we see that, for an RF mixer

$$\left[S^{\mathrm{M,RF}}\right] = \begin{bmatrix} S^{\mathrm{IF}}_{11} & a^*_{\mathrm{LO}} S^{\mathrm{IF}}_{12} \\ a_{\mathrm{LO}} S^{\mathrm{IF}}_{21} & S^{\mathrm{IF}}_{22} \end{bmatrix}. \tag{10}$$

Identifying Maas' port 1 with the mixer's image port, we can rewrite [3, eq. (4.88)] for an image mixer as

$$\begin{bmatrix} b^*_{\mathrm{IM}} \\ b_{\mathrm{IF}} \end{bmatrix} = \left[S^{\mathrm{M,IM}}\right] \begin{bmatrix} a^*_{\mathrm{IM}} \\ a_{\mathrm{IF}} \end{bmatrix} \equiv \begin{bmatrix} S^{\mathrm{M}}_{-1,-1} & S^{\mathrm{M}}_{-1,0} \\ S^{\mathrm{M}}_{0,-1} & S^{\mathrm{M}}_{0,0} \end{bmatrix} \begin{bmatrix} a^*_{\mathrm{IM}} \\ a_{\mathrm{IF}} \end{bmatrix}. \tag{11}$$

Note that Maas defined port 1 as the image port, and port 2 as the IF port in [3, eq. (4.88)], which gives rise to the reversal of the wave coefficients in the vectors in (5) and (11). Comparing (5) and (11), we see that, for an image mixer

$$\left[S^{\mathrm{M,IM}}\right] = \begin{bmatrix} S^{\mathrm{IF}}_{22} & a^*_{\mathrm{LO}} S^{\mathrm{IF}}_{21} \\ a_{\mathrm{LO}} S^{\mathrm{IF}}_{12} & S^{\mathrm{IF}}_{11} \end{bmatrix}. \tag{12}$$

Appendix II
Relationship to Large-Signal Scattering Functions

Verspecht *et al.* [9]–[11] introduced a linearization of a "large-signal scattering function" relating signals at a set harmonic frequencies.[3] Part of the utility of this linearization is that its parameters can be determined by artificial neural networks from large-signal network-analyzer measurements.

The linearization uses two complex Jacobian-like matrices $[S_{\mathrm{V}}]$ and $[S'_{\mathrm{V}}]$ to map the small-signal input vector of complex wave coefficients A into the small-signal output vector of wave coefficients B with [11] as follows:

$$B \approx [S_{\mathrm{V}}]A + [S'_{\mathrm{V}}]A^*. \tag{13}$$

If we eliminate all of the elements of $[S_{\mathrm{V}}]$ and $[S'_{\mathrm{V}}]$, except those relating the IF at the input of a mixer and the RF (or image) frequency at the output of a mixer, we can write $A = (a_{\mathrm{IF}}, a_{\mathrm{RF}})^{\mathrm{T}}$ and $B = (b_{\mathrm{IF}}, b_{\mathrm{RF}})^{\mathrm{T}}$, where the superscript T indicates the transpose. Comparing (3) and (13), we see that, for an RF mixer

$$[S_{\mathrm{V}}] = \begin{bmatrix} S^{\mathrm{IF}}_{11} & a^*_{\mathrm{LO}} S^{\mathrm{IF}}_{12} \\ a_{\mathrm{LO}} S^{\mathrm{IF}}_{21} & S^{\mathrm{IF}}_{22} \end{bmatrix} \quad [S'_{\mathrm{V}}] = 0. \tag{14}$$

For an image mixer with $A = (a_{\mathrm{IF}}, a_{\mathrm{IM}})^{\mathrm{T}}$, and $B = (b_{\mathrm{IF}}, b_{\mathrm{IM}})^{\mathrm{T}}$, we have, from (5) and (13)

$$[S_{\mathrm{V}}] = \begin{bmatrix} S^{\mathrm{IF}}_{11} & 0 \\ 0 & S^{\mathrm{IF}*}_{22} \end{bmatrix}$$
$$[S'_{\mathrm{V}}] = \begin{bmatrix} 0 & a_{\mathrm{LO}} S^{\mathrm{IF}}_{12} \\ a_{\mathrm{LO}} S^{\mathrm{IF}*}_{21} & 0 \end{bmatrix}. \tag{15}$$

Acknowledgment

The authors thank J. Verspecht, for help with Appendix II and S. Maas, for his helpful comments.

[3]The linearization of [9]–[11] should not be confused with the "large-signal scattering parameters" of [12]. The large-signal scattering parameters of [12] relate vectors of incident and reflected large-signal wave coefficients $\mathbf{A}$ and $\mathbf{B}$ with a scattering matrix $[S_{\mathrm{J}}]$ via $\mathbf{B} = [S_{\mathrm{J}}]\mathbf{A}$.

REFERENCES

[1] J. Dunsmore, S. Hubert, and D. F. Williams, "Vector mixer characterization for high-side LO cases," presented at the IEEE MTT-S Int. Microwave Symp., 2004 .

[2] H. C. Torrey, C. A. Whitmer, and S. Goudsmit, *Crystal Rectifiers*. New York: McGraw-Hill, 1948.

[3] S. Maas, *Microwave Mixers*. Boston, MA: Artech House, 1992.

[4] R. B. Marks and D. F. Williams, "A general waveguide circuit theory," *J. Res. Nat. Inst. Standards Technol.*, vol. 97, no. 5, pp. 533–562, Sep.–Oct. 1992.

[5] J. Dunsmore, "Novel method for vector mixer characterization and mixer test system vector error correction," in *IEEE MTT-S Int. Microwave Symp. Dig.*, Jun. 2–7, 2002, pp. 1833–1836.

[6] A. Cidronali, K. C. Gupta, J. Jargon, K. A. Remley, D. DeGroot, and G. Manes, "Extraction of conversion matrices for P-HEMT's based on vectorial large-signal measurements," in *IEEE MTT-S Int. Microwave Symp. Dig.*, vol. 2, Jun. 8–13, 2003, pp. 777–780.

[7] W. Van Moer and Y. Rolain, "Proving the usefulness of a 3-port nonlinear vectorial network analyzer through mixer measurements," in *IEEE MTT-S Int. Microwave Symp. Dig.*, vol. 3, Jun. 8–13, 2003, pp. 1647–1650.

[8] R. F. Bauer and P. Penfield, "De-embedding and unterminating," *IEEE Trans. Microw. Theory Tech.*, vol. MTT-22, no. 3, pp. 282–288, Mar. 1974.

[9] J. Verspecht, M. Vanden Bossche, and F. Verbeyst, "Characterizing components under large signal excitation: Defining sensible 'large signal S-parameters'," in *49th ARFTG Conf. Dig.*, 1997, pp. 109–117.

[10] J. Verspecht and P. Van Esch, "Accurately characterizing hard nonlinear behavior of microwave components with the nonlinear network measurement system: Introducing 'nonlinear scattering functions'," presented at the 5th Int. Integrated Nonlinear Microwave and Millimeter Wave Circuits Workshop, 1998.

[11] J. Verspecht, "Scattering functions for nonlinear behavioral modeling in the frequency domain," presented at the IEEE MTT-S Int. Microwave Symp. Workshop, Jun. 2003.

[12] J. A. Jargon, K. C. Gupta, D. Schreurs, and D. C. DeGroot, "Developing frequency-domain models for nonlinear circuits based on large-signal measurements," in *Proc. XXVIIth Int. Union Radio Sci. Gen. Assembly*, Maastricht, The Netherlands, Aug. 2002 [CD-ROM A1.0.6].

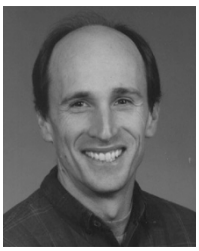

Dylan F. Williams (M'80–SM'90–F'02) received the Ph.D. degree in electrical engineering from the University of California at Berkeley, in 1986.

In 1989, he joined the Electromagnetic Fields Division, National Institute of Standards and Technology (NIST), Boulder, CO, where he develops metrology for the characterization of monolithic microwave integrated circuits (MMICs) and electronic interconnects. He has authored or coauthored over 80 technical papers.

Dr. Williams is an associate editor for the IEEE TRANSACTIONS ON MICROWAVE THEORY AND TECHNIQUES. He was the recipient of the Department of Commerce Bronze and Silver Medals, the Electrical Engineering Laboratory's Outstanding Paper Award, two Automatic RF Techniques Group (ARFTG) Best Paper Awards, the ARFTG Automated Measurements Technology Award, and the IEEE Morris E. Leeds Award.

Fabien Ndagijimana received the Ph.D. degree (with a specialization in microwave and optoelectronics) from the Institut National Polytechnique de Grenoble (INPG), Grenoble, France, in 1990.

He then joined the faculty of electrical engineering as an Associate Professor with the Ecole Nationale Supérieure d'Electronique et de Radioélectricité de Grenoble (ENSERG), Grenoble, France, where he teaches microwave techniques and electromagnetic modeling. He is currently a Professor with the Université Joseph Fourier, Grenoble, France, and the Institut Universitaire de Technologie (IUT), Grenoble, France. His research activity with the Institut de Microélectronique d'Electromagnétisme et Photonique (IMEP) focuses on the characterization and electromagnetic modeling of microwave and high-speed circuits, and their integration on silicon/silicon-on-insulator (SOI) technologies.

Kate A. Remley (S'92–M'99) was born in Ann Arbor, MI, in 1959. She received the Ph.D. degree in electrical and computer engineering from Oregon State University, Corvallis, in 1999.

From 1983 to 1992, she was a Broadcast Engineer in Eugene, OR. From 1989 to 1991, she was Chief Engineer of an AM/FM broadcast station. In 1999, she joined the Radio-Frequency Technology Division, National Institute of Standards and Technology (NIST), Boulder, CO, as an Electronics Engineer. Her research activities focus on development of metrology for wireless systems, and characterizing the link between nonlinear circuits and system performance.

Dr. Remley was the recipient of the Department of Commerce Silver Medal and the Automatic RF Techniques Group (ARFTG) Best Paper Award.

Joel A. Dunsmore (M'83) received the B.S.E.E. and M.S.E.E. degrees from Oregon State University, Corvallis, in 1982 and (1983, respectively.

He was with Agilent Technologies (formerly Hewlett-Packard), Sonoma County, CA. He is a Senior Design Engineer with the Component Test Division, Agilent Technologies, Santa Rosa, CA. He was a principle contributor to the HP 8753 and HP 8720 family of network analyzers, responsible for RF and microwave-circuit designs in these products. Recently, he has been involved in the area of nonlinear test including differential devices and mixer measurements. He has authored or coauthored numerous papers on measurement technology. He holds 11 U.S. patents related to this work. He has been a consultant on measurement applications. He has taught electrical-circuit fundamentals and presented several short courses and seminars through the Automatic RF Techniques Group (ARFTG), the IEEE Microwave Theory and Techniques Society (IEEE MTT-S), the IEEE Electromagnetic Compatibility (EMC) Society, and Agilent Technologies.

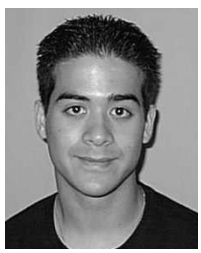

Sean Hubert received the B.S. degree in computer science from the University of California at Berkeley, in 2000.

Since then, he has been a Research and Development Software Engineer with Agilent Technologies, Santa Rosa, CA. With Agilent Technologies, he was a Principal Developer on several projects including filter tuning software (FTS), frequency converter application (FCA), and the performance network analyzer (PNA) firmware. He holds several U.S. patents for these applications.